Cancer Research

2-Hydroxyglutarate-Mediated Autophagy of the Endoplasmic Reticulum Leads to an Unusual Downregulation of Phospholipid Biosynthesis in Mutant IDH1 Gliomas

Pavithra Viswanath[1], Marina Radoul[1], Jose Luis Izquierdo-Garcia[2,3], Wei Qiang Ong[4], Hema Artee Luchman[5], J. Gregory Cairncross[6], Bo Huang[4], Russell O. Pieper[7], Joanna J. Phillips[7], and Sabrina M. Ronen[1]

Abstract

Tumor metabolism is reprogrammed to meet the demands of proliferating cancer cells. In particular, cancer cells upregulate synthesis of the membrane phospholipids phosphatidylcholine (PtdCho) and phosphatidylethanolamine (PtdE) in order to allow for rapid membrane turnover. Nonetheless, we show here that, in mutant isocitrate dehydrogenase 1 (IDHmut) gliomas, which produce the oncometabolite 2-hydroxyglutarate (2-HG), PtdCho and PtdE biosynthesis is downregulated and results in lower levels of both phospholipids when compared with wild-type IDH1 cells. 2-HG inhibited collagen-4-prolyl hydroxylase activity, leading to accumulation of misfolded procollagen-IV in the endoplasmic reticulum (ER) of both genetically engineered and patient-derived IDHmut glioma models. The resulting ER stress triggered increased expression of FAM134b, which mediated autophagic degradation of the ER (ER-phagy) and a reduction in the ER area. Because the ER is the site of phospholipid synthesis, ER-phagy led to reduced PtdCho and PtdE biosynthesis. Inhibition of ER-phagy via pharmacological or molecular approaches restored phospholipid biosynthesis in IDHmut glioma cells, triggered apoptotic cell death, inhibited tumor growth, and prolonged the survival of orthotopic IDHmut glioma-bearing mice, pointing to a potential therapeutic opportunity. Glioma patient biopsies also exhibited increased ER-phagy and downregulation of PtdCho and PtdE levels in IDHmut samples compared with wild-type, clinically validating our observations. Collectively, this study provides detailed and clinically relevant insights into the functional link between oncometabolite-driven ER-phagy and phospholipid biosynthesis in IDHmut gliomas.

Significance: Downregulation of phospholipid biosynthesis via ER-phagy is essential for proliferation and clonogenicity of mutant IDH1 gliomas, a finding with immediate therapeutic implications. *Cancer Res; 78(9); 2290–304. ©2018 AACR.*

Introduction

Mutations in isocitrate dehydrogenase 1 (*IDH1*) are characteristic of 70% to 90% of low-grade gliomas (1). The wild-type IDH1 (IDHwt) enzyme converts isocitrate to α-ketoglutarate (α-KG) while mutant IDH1 (IDHmut) converts α-KG to 2-hydroxyglutarate (2-HG; ref. 1). 2-HG is an oncometabolite that inhibits the activity of α-KG–dependent dioxygenases including prolyl hydroxylases, histone demethylases, and the TET family of 5-methylcytosine hydroxylases. The resulting alterations in cell signaling and epigenetics ultimately drive tumorigenesis (1, 2).

In addition, IDHmut cells undergo a broad reprogramming of cellular metabolism, extending beyond 2-HG production (3). Specifically, when compared with IDHwt, IDHmut cells silence lactate dehydrogenase A expression and concomitant lactate production (4, 5), and downregulate pyruvate dehydrogenase activity reducing flux to the tricarboxylic acid cycle (6). Studies have also reported alterations in glutaminolysis (7) and cellular redox status (8). Several of these metabolic changes can potentially be exploited for therapy (6–8), pointing to the importance of metabolic reprogramming in sustaining IDHmut cell proliferation.

Another important metabolic pathway that has not been extensively investigated in IDHmut gliomas is that of phospholipid metabolism. Phosphatidylcholine (PtdCho) and phosphatidylethanolamine (PtdE) are structural components of cell membranes and are quantitatively the most abundant phospholipids in the cell (9, 10). Proliferating cancer cells have a higher demand for phospholipids due to rapid membrane turnover (11, 12) and, as a result, PtdCho and PtdE biosynthesis is activated (12–15). The biosynthetic pathways (Fig. 1A) begin with choline and

[1]Department of Radiology and Biomedical Imaging, University of California San Francisco, San Francisco, California. [2]Centro Nacional de Investigaciones Cardiovasculares (CNIC), Madrid, Spain. [3]CIBER de Enfermedades Respiratorias (CIBERES), Madrid, Spain. [4]Department of Pharmaceutical Chemistry, University of California San Francisco, San Francisco, California. [5]Department of Cell Biology and Anatomy and Hotchkiss Brain Institute, University of Calgary, Calgary, Alberta, Canada. [6]Department of Clinical Neurosciences and Southern Alberta Cancer Research Institute, University of Calgary, Calgary, Alberta, Canada. [7]Department of Neurological Surgery, Helen Diller Research Center, University of California San Francisco, San Francisco, California.

Note: Supplementary data for this article are available at Cancer Research Online (http://cancerres.aacrjournals.org/).

Corresponding Author: Sabrina M. Ronen, University of California San Francisco, 1700 4th Street, Box 2532, Byers Hall 3rd Floor, Suite, San Francisco, CA 94158. Phone: 415-514-4839; Fax: 415-514-4839; E-mail: sabrina.ronen@ucsf.edu

doi: 10.1158/0008-5472.CAN-17-2926

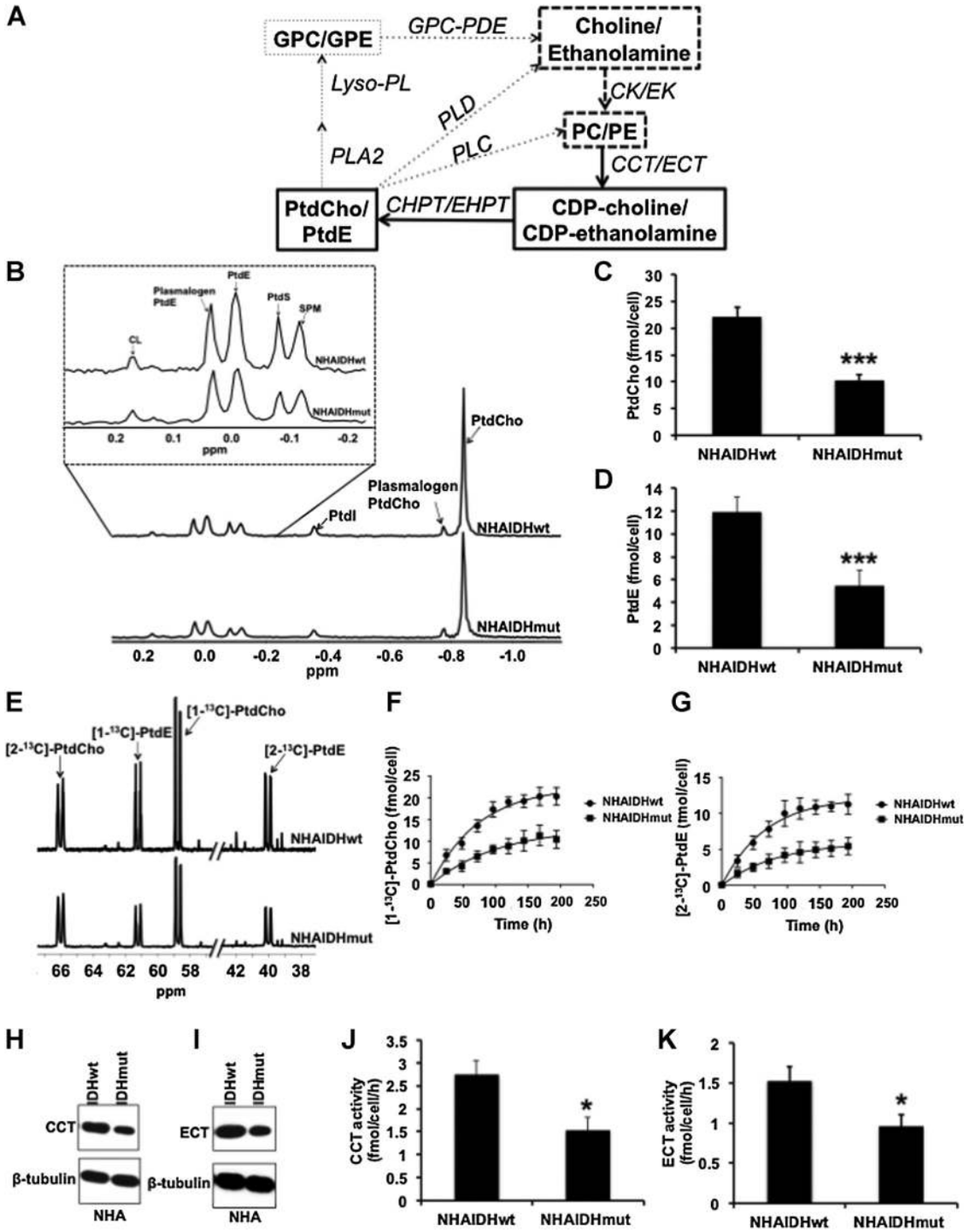

Figure 1.

Phospholipid biosynthesis is downregulated in IDHmut glioma cells. **A,** PtdCho and PtdE biosynthetic pathways. CK, choline kinase; EK, ethanolamine kinase; CCT, CTP:PC cytidylyltransferase; ECT, CTP:PE cytidylyltransferase; CHPT, choline phosphotransferase; EHPT, ethanolamine phosphotransferase; PLA2, phospholipase A2; Lyso-PL, lyso-phospholipase; GPC-PDE, glycerophosphocholine. Dashed lines, reactions occurring in the cytosol; thick lines, those reactions occurring in the ER; dotted lines, the phospholipid breakdown pathway. **B,** ^{31}P-MR spectra of the lipid fraction of cell extracts. The inset shows expansion of the 0.2 to −0.2 ppm region. CL, cardiolipin; PtdI, phosphatidylinositol; PtdS, phosphatidylserine; SPM, sphingomyelin; plasmalogen PtdCho, PtdE, ether phospholipids. PtdCho (**C**) and PtdE (**D**) levels in the NHA model. **E,** Representative ^{13}C-MR spectra of the lipid fraction of cell extracts. Nonlinear kinetic fit of [1-^{13}C]-PtdCho (**F**) and [2-^{13}C]-PtdE (**G**) synthesis in the NHA model. Western blots of CCT (**H**) and ECT (**I**) expression in the NHA model. CCT activity (**J**) and ECT activity (**K**) in the NHA model. *, $P < 0.05$; ***, $P < 0.005$.

ethanolamine import, followed by cytosolic phosphorylation to phosphocholine (PC) and phosphoethanolamine (PE) via choline kinase and ethanolamine kinase (16, 17). PC and PE are then converted to CDP-choline and CDP-ethanolamine by CTP:PC cytidylyltransferase (CCT) and CTP:PE cytidylyltransferase (ECT). CCT and ECT are the rate-limiting steps in PtdCho and PtdE biosynthesis (14, 16, 18) and, importantly, their active forms are associated with the ER (9, 19, 20). Finally, choline phosphotransferase and ethanolamine phosphotransferase catalyze the production of PtdCho and PtdE, again in the ER (20).

Consistent with increased phospholipid synthesis, magnetic resonance spectroscopy (MRS) studies have demonstrated an increase in PC and PE, the precursors of PtdCho and PtdE, in most types of cancer (12, 21–23). Interestingly however, and counter to these findings, studies in IDHmut cells have reported reduced PC (24, 25) and PE (26) relative to IDHwt pointing to a potentially unusual reprogramming of phospholipid biosynthesis in IDHmut cells.

The goal of this study was therefore to investigate PtdCho and PtdE biosynthesis in IDHmut glioma cells. Our study indicated that 2-HG downregulated PtdCho and PtdE biosynthesis and steady-state levels in IDHmut cells relative to IDHwt. This effect was mediated by autophagic degradation of the ER (ER-phagy), the site of CCT and ECT activity and phospholipid biosynthesis. Importantly, we confirmed our findings in IDHmut glioma patient biopsies, thereby validating the clinical relevance of our study. Furthermore, inhibition of ER-phagy restored phospholipid levels and triggered apoptosis *in vitro* and *in vivo*, identifying this metabolic reprogramming as essential for IDHmut cell survival.

Materials and Methods

Cell culture

U87 and NHA cells expressing IDHwt (U87IDHwt/NHAIDHwt) or IDH1 R132H-mutant enzyme (U87IDHmut/NHAIDHmut) were generated and maintained as described previously (25). BT54 neurospheres were provided by H.A. Luchman and J.G. Cairncross and maintained as described previously (27). BT54 proliferation was assayed as described (6). Cells were used for studies between passages 15 and 30. All cell lines were routinely tested for *Mycoplasma* contamination, authenticated by short tandem repeat fingerprinting (Cell Line Genetics) and used for studies within 6 months of authentication. Treatment with D-2-HG (Sigma-Aldrich) was with 1 mmol/L for 24 hours, AGI-5198 with 10 μmol/L for 72 hours, bafilomycin A1 (BAF) with 50 nmol/L for 16 hours, chloroquine (CQ) with 50 μmol/L for 16 hours, ethyl-3,4-dihydroxybenzoate (EDHB) with 270 μmol/L for 24 hours. For kinetic analysis of the effect of CQ and BAF, cells were treated for 4 and 16 hours. DMSO was used as vehicle control.

RNA interference

SMARTpool siRNAs (Dharmacon) against human FAM134b (M-016936-01), Atg5 (M-004374-04), Atg7 (M-020112-01), and non-targeting siRNA pool #2 (D-001206-14-05) were transfected according to the manufacturer's instructions.

MRS studies

Metabolites were extracted by dual-phase extraction (25). ^{1}H-MR spectra (1D ZGPR, 90°flip angle, 3-second relaxation delay, 256 acquisitions), proton-decoupled ^{13}C-MR spectra (30° flip angle, 3-second relaxation delay, and 2,048 acquisitions) and proton-decoupled ^{31}P-MR spectra (30° flip angle, 2.6-second relaxation delay, 1,440 scans) were obtained using a 500 MHz spectrometer (Bruker) equipped with a Triple Resonance CryoProbe (6). Peak integrals were quantified using Mnova, corrected for saturation and normalized to cell number and an external reference (trimethylsilylpropionate for ^{1}H- and ^{13}C-MR and methylene diphosphonic acid for ^{31}P).

For measurement of *de novo* PtdCho and PtdE biosynthesis, cells were cultured in medium containing 56 μmol/L [1,2-^{13}C]-choline and 56 μmol/L [1,2-^{13}C]-ethanolamine (Sigma-Aldrich) for various time points. Kinetic build-up of ^{13}C-Ptdcho and -PtdE was analyzed by nonlinear regression (GraphPad Prism) using the equation $^{13C}\text{PtdCho}(t) = A\,(1 - e^{-kt})$, where ^{13C}PtdCho represents ^{13}C-PtdCho at time point t, A represents the asymptotic value of the ^{13}C-labeled pool of PtdCho and k is the pseudo–first-order rate constant for PtdCho synthesis. A similar equation was used for PtdE synthesis.

CCT activity was determined as described (28). For ECT activity, cells were lysed (50 mmol/L HEPES, pH 7, 5 mmol/L EDTA, 5 mmol/L EGTA) and combined with reaction mix (50 mmol/L Tris-HCl, pH 8, 5 mmol/L DTT, 10 mmol/L cytidine triphosphate, 5 mmol/L PE, 25 mmol/L $MgCl_2$). Proton-decoupled ^{31}P-MR spectra (30° flip angle, 2.6-second relaxation delay, 128 transients) were acquired every 5 minutes and ECT activity determined by linear regression of the kinetics of CDP-ethanolamine production.

Western blotting

Protein was probed for pan-cadherin (4068), COX-IV (4850), NUP98 (2598), Atg5 (12994), Atg7 (8558), cleaved PARP (5625) from Cell Signaling, for CCTα (Pcyt1A, ab109263), ECT (Pcyt2, ab15053), calnexin (ab22595), golgin-97 (ab84340), FAM134b (ab151755), collagen-IV (ab6586) from Abcam and for LC3B (0231-100) from Nanotools. β-Actin (4970), GAPDH (2118) and β-tubulin (2128) from Cell Signaling were used as loading control.

Immunofluorescence

Cells were seeded on Lab-Tek-II Coverglass (ThermoScientific) and stained with primary antibody (anti-calnexin, ab22595, Abcam, for STORM imaging and anti-calnexin, ab66332, Abcam plus anti-LC3B, 0231-100, Nanotools, for confocal imaging) and then with secondary antibody (Alexa647 for STORM imaging and Alexa488 plus Alexa647 for confocal imaging).

STORM imaging

Imaging was performed using a custom-built Nikon Eclipse Ti-E inverted microscope. 405nm and 640nm lasers (OBIS640, Coherent) were focused at the back focal plane of the UPlanSApo 1.4NA 100× objective (Olympus). Images were recorded with an electron-multiplying CCD camera (iXon+ DU897E-C20-BV, Andor). A quadband dichroic mirror (ZT405/488/561/640rpc) and band-pass filter (ZET405/488/561/647m for 405 nm and ET700/75 nm for 640 nm) separated the fluorescence emission from the excitation light. Images were recorded at a frame rate of 60 Hz. Data acquisition and analysis were performed as described (29). The total number of calnexin localization points was used as a measure of ER area for each cell.

Confocal microscopy

Cells were treated with 50 nmol/L BAF for 4 hours prior to imaging since endogenous LC3B levels were otherwise too low. Images were acquired using a Nikon Eclipse Ti microscope equipped with an Andor Zyla sCMOS camera.

Autophagic flux determination

Autophagic flux was quantified by measuring LC3-II levels by immunoblotting in the presence of BAF as recommended (30). The normalized densitometric value of LC3-II in control samples was subtracted from the corresponding BAF-treated samples to calculate the autophagic flux.

Coimmunoprecipitation

Cells were lysed (50 mmol/L Tris-HCl pH 7.8, 1% Triton X-100, 300 mmol/L NaCl, 5 mmol/L EDTA), supernatant incubated with anti-calnexin antibody (ab66332, Abcam) and protein-G beads and bound proteins examined by immunoblotting.

Hydroxyproline assay

Hydroxyproline content was determined spectrophotometrically (30).

Procollagen-IV fractionation

Cells were lysed (50 mmol/L Tris-HCl, pH 8, 150 mmol/L NaCl, 5 mmol/L EDTA, 1% NP-40), centrifuged at 14,000 rpm for 20 minutes to separate supernatant (detergent-soluble) and pellet (detergent-insoluble) fractions for immunoblotting.

Caspase activity and cell size

Caspase activity (ab39401, Abcam) and cell size (F-13838, Thermo-Fisher) were measured using commercial kits.

Animal studies

All animal studies were approved by the University of California Institutional Animal Care and Use Committee (IACUC) under protocol number AN101013. U87IDHwt or U87IDHmut cells (3×10^5 cells/10 μL) were intracranially injected into athymic nu/nu mice. Once the tumor reached 2 to 3 mm as assessed by MR imaging, this time point was considered day zero (D0). Mice with each tumor type were randomly divided into two groups and treated once daily intraperitoneally with saline ($n = 5$ for U87IDHwt, $n = 6$ for U87IDHmut) or 60 mg/kg CQ ($n = 5$ for U87IDHwt, $n = 7$ for U87IDHmut). In order to obtain tumor tissue for analysis, CQ-treated mice were sacrificed at D21 when U87IDHmut tumors had shrunk to below their size at D0. Control animals were treated until they had to be sacrificed per IACUC guidelines.

MR imaging was performed on a 14.1T vertical MR system (Agilent), equipped with a single-channel 1H coil. For T2-weighted imaging, images were acquired using a multislice spin–echo sequence: time-to-echo: 20 ms; repetition time: 1,200 ms; field of view: 25×25 mm^2; matrix: 512×256; slice thickness: 1.0 mm; number of averages: 2. Tumor contours were drawn manually and tumor volume determined as a sum of the areas multiplied by slice thickness using in-house MR software (SIVIC).

Patient samples

Flash-frozen human tumor tissue, with no patient-identifying information, was obtained in compliance with written informed consent policy from the UCSF Brain Tumor Center Biorepository and Pathology Core. Sample use was approved by the Committee on Human Research at UCSF and research was approved by the Institutional Review Board at UCSF according to ethical guidelines established by the U.S. Common Rule. Immunohistochemistry for LC3-II (0231-100, Nanotools) was performed on tissue microarrays using a Ventana Benchmark XT automated slide preparation system.

Statistical analysis

All experiments were performed on a minimum of 5 samples and results presented as mean ± SD. For biopsy studies, 4 IDHwt and 3 IDHmut samples were tested. Statistical significance was assessed using an unpaired Student t test assuming unequal variance with $P < 0.05$ considered significant (*, $P < 0.05$; **, $P < 0.01$; ***, $P < 0.005$). Analysis of mRNA expression data from IDHwt and IDHmut low-grade glioma patient biopsies from The Cancer Genome Atlas (TCGA) database was performed as described previously (4).

Results

Phospholipid biosynthesis is downregulated in IDHmut glioma cells

We investigated two genetically engineered models, a U87 model and an immortalized normal human astrocyte (NHA) model, expressing IDHwt or IDH1 R132H-mutant enzyme (Supplementary Fig. S1A–S1B; ref. 25). First, we used ^{31}P-MRS (Fig. 1B) to determine steady-state PtdCho and PtdE levels and found that both phospholipids were significantly reduced in IDHmut cells (Fig. 1C–D; Supplementary Fig. S1C–S1D). Using ^{13}C-MRS (Fig. 1E), we then monitored phospholipid biosynthesis by labeling cells with [1,2-^{13}C]-choline and [1,2-^{13}C]-ethanolamine until *de novo* synthesized ^{13}C-PtdCho and -PtdE reached total steady-state levels (as determined by comparison with the ^{31}P-MRS data). PtdCho and PtdE biosynthetic rates were reduced in IDHmut cells (Fig. 1F–G; Supplementary Fig. S1E–S1F). The pseudo–first-order rate constant for PtdCho synthesis dropped significantly by 38% in the NHA model from 0.013 ± 0.001/h in NHAIDHwt to 0.008 ± 0.001/h in NHAIDHmut and by 41% from 0.033 ± 0.001/h in U87IDHwt to 0.019 ± 0.002/h in U87IDHmut. The pseudo–first-order rate constant for PtdE synthesis also dropped significantly by 43% from 0.012 ± 0.001/h to 0.007 ± 0.001/h in the NHA model and by 45% from 0.029 ± 0.001/h to 0.016 ± 0.002/h in the U87 model.

Next, we examined expression of CCT and ECT, the rate-limiting enzymes in PtdCho and PtdE biosynthesis. In the NHA model, CCT expression dropped significantly by 42% (Fig. 1H) and ECT expression by 38% (Fig. 1I) with similar findings in the U87 model (Supplementary Fig. S1G–1H). We also measured CCT and ECT activities using ^{31}P-MRS–based activity assays (Supplementary Fig. S1I–S1J), and found a significant reduction in their activities in IDHmut compared with IDHwt (Fig. 1J–K for NHA and Supplementary Fig. S1K–S1L for U87).

2-HG is responsible for the downregulation of phospholipid biosynthesis in IDHmut glioma cells

Next, we wanted to confirm the link between 2-HG and our metabolic observations. To that end, we examined phospholipid biosynthesis in IDHwt cells incubated with 2-HG (to cause intracellular accumulation of 2-HG), or in IDHmut cells treated

with the IDHmut inhibitor AGI-5198 (to cause depletion of 2-HG; ref. 31). Using ^{1}H-MRS, we confirmed that our treatments modulated 2-HG as expected (Fig. 2A; Supplementary Fig. S2A).

Consistent with a link between 2-HG and phospholipid biosynthesis, steady-state PtdCho and PtdE dropped in IDHwt cells incubated with 2-HG to levels similar to those observed in IDHmut cells in both NHA (Fig. 2B–C) and U87 (Supplementary Fig. S2B–S2C) models. Conversely, depletion of 2-HG by treatment of IDHmut cells with AGI-5198 restored PtdCho and PtdE to levels akin to those observed in IDHwt cells (Fig. 2B–C; Supplementary Fig. S2B–S2C). Furthermore, 2-HG incubation of IDHwt cells reduced the pseudo–first-order rate constant of *de novo* PtdCho and PtdE synthesis to levels observed in IDHmut cells while treatment of IDHmut cells with AGI-5198 restored the rate constant to IDHwt levels (Fig. 2D–E; Supplementary Fig. S2D–S2E). Expression of CCT (Fig. 2F; Supplementary Fig. S2F) and ECT (Fig. 2G; Supplementary Fig. S2G) as well as their activities (Fig. 2H–I; Supplementary Fig. S2H–S2I) also dropped to IDHmut levels in 2-HG–treated IDHwt cells and were restored to IDHwt levels in AGI-5198–treated IDHmut cells.

2-HG induces a reduction in ER area via autophagic degradation of the ER in IDHmut glioma cells

CCT and ECT are localized to the ER, which is the principal site for phospholipid biosynthesis (9, 10, 19, 20, 32). We therefore questioned whether ER area was altered in IDHmut cells. Super-resolution stochastic optical reconstruction microscopic (STORM) imaging of the ER membrane marker calnexin revealed a striking reduction in ER area in IDHmut cells relative to IDHwt in a manner associated with 2-HG in both NHA (Fig. 3A and B) and U87 (Supplementary Fig. S3A–S3B) models. These findings were also confirmed by Western blotting in both NHA and U87 models (Supplementary Fig. S3C).

To rule out the possibility of nonspecific organelle turnover in IDHmut cells, we examined expression of other major organelle markers and found no change in plasma membrane (pan-cadherin), golgi (golgin-97), mitochondria (cytochrome c oxidase IV, COX-IV), and nuclear envelope (NUP98) markers (Supplementary Fig. S3D–S3K). Finally, because PtdCho and PtdE are major structural components of the plasma membrane, we examined cell size (Supplementary Fig. S3L–S3M) and found no difference in our models.

Autophagy of the ER ("ER-phagy") can regulate ER area (33–35), and so we questioned whether ER-phagy was activated in IDHmut cells. FAM134b is an ER-resident protein that binds to the autophagosomal membrane protein LC3-II and mediates autophagosome recruitment to the ER, thereby initiating ER-phagy (33). FAM134b expression was higher in IDHmut cells, in a manner linked to the presence of 2-HG (Fig. 3C; Supplementary Fig. S4A). To quantify autophagic flux, we then measured LC3-II levels in the presence of the lysosomal inhibitor BAF (an increase in LC3-II in the presence of BAF indicates increased autophagic flux rather than blocked autophagosome turnover; ref. 36). Autophagic flux was higher in IDHmut cells in a 2-HG–dependent manner (Fig. 3D; Supplementary Fig. S4B).

To further confirm ER-phagy, we performed coimmunoprecipitation assays and found a direct interaction between calnexin, the ER marker, and endogenous LC3-II in IDHmut cells or 2-HG–treated IDHwt cells, but not in IDHwt cells or in AGI-5198–treated IDHmut cells (Fig. 3E; Supplementary Fig. S4C). Furthermore, confocal microscopy showed colocalization of calnexin with endogenous LC3B only in IDHmut cells and in 2-HG–treated IDHwt cells (Supplementary Fig. S4D).

ER-phagy is activated in response to accumulation of misfolded proteins in the ER (34, 35). 2-HG has been reported to inhibit collagen prolyl-4-hydroxylase (C-4-PH) activity (37, 38), leading to accumulation of misfolded collagen-IV (38). To assess folded collagen in our models, we therefore examined hydroxyproline levels and found a significant reduction in IDHmut cells relative to IDHwt (Fig. 3F; Supplementary Fig. S4E). Furthermore, procollagen-IV was largely detergent-insoluble in IDHmut cells relative to IDHwt (Fig. 3G; Supplementary Fig. S4F). Incubation of IDHwt cells with 2-HG shifted procollagen-IV to the detergent-insoluble fraction, while treatment of IDHmut cells with AGI-5198 increased detergent-soluble procollagen-IV, indicating that 2-HG induced accumulation of misfolded procollagen-IV in the ER.

To further confirm that C-4PH inhibition was linked to ER-phagy and reduced phospholipid biosynthesis, we treated IDHwt cells with the prolyl hydroxylase inhibitor ethyl-3,4-dihydroxybenzoate (EDHB; ref. 39). EDHB induced accumulation of misfolded procollagen IV in IDHwt cells (Supplementary Fig. S4G–S4H). Concomitantly, ER area was reduced (Supplementary Fig. S4I–S4J) and coimmunoprecipitation assays showed a direct interaction between calnexin and endogenous LC3-II in EDHB-treated IDHwt cells (Supplementary Fig. S4K–S4L), consistent with induction of ER-phagy only when C-4PH is inhibited. Furthermore, EDHB treatment also reduced PtdCho (Supplementary Fig. S4M) and PtdE (Supplementary Fig. S4N) levels in IDHwt cells.

An alternative cellular response to misfolded protein accumulation in the ER is induction of apoptosis by the transcription factor CHOP (40). Caspase activity was below detection in our models and there was no difference in CHOP expression (Supplementary Fig. S4O–S4P), ruling out apoptosis. Instead, our data indicated that misfolded procollagen-IV triggered ER-phagy in IDHmut cells.

Silencing FAM134b, Atg5, or Atg7 restores ER area and phospholipid levels in IDHmut glioma cells

To confirm that ER-phagy was linked to phospholipid biosynthesis, we used RNA interference in IDHmut cells to silence FAM134b (Supplementary Fig. S5A–S5B) and thus prevent autophagosome recruitment to the ER. We also silenced the autophagy proteins Atg5 and Atg7 that are indispensable for autophagosome formation and autophagic flux (Supplementary Fig. S5A–S5B; ref. 41).

First, we confirmed that silencing Atg5 or Atg7 blocked autophagic flux (Supplementary Fig. S5C–S5D) and abrogated coimmunoprecipitation of LC3-II with calnexin (Supplementary Fig. S5E–S5F). We then investigated the impact on ER area and found that it was significantly increased as seen by STORM imaging (Fig. 4A). Importantly, silencing autophagy also increased CCT expression and activity, ECT expression and activity, PtdCho and PtdE in both NHA (Fig. 4B–G) and U87 (Supplementary Fig. S5G–S5L) models, confirming the link between ER-phagy and phospholipid metabolism in IDHmut cells (Fig. 4H).

Furthermore, silencing FAM134b, Atg5, or Atg7 induced caspase activity (Fig. 4I; Supplementary Fig. S5M) and cleaved PARP (Supplementary Fig. S5N–S5O), indicating induction of apoptosis. It also significantly inhibited clonogenicity (Fig. 4J; Supplementary Fig. S5P), indicating that disrupting ER-phagy was detrimental to IDHmut cells.

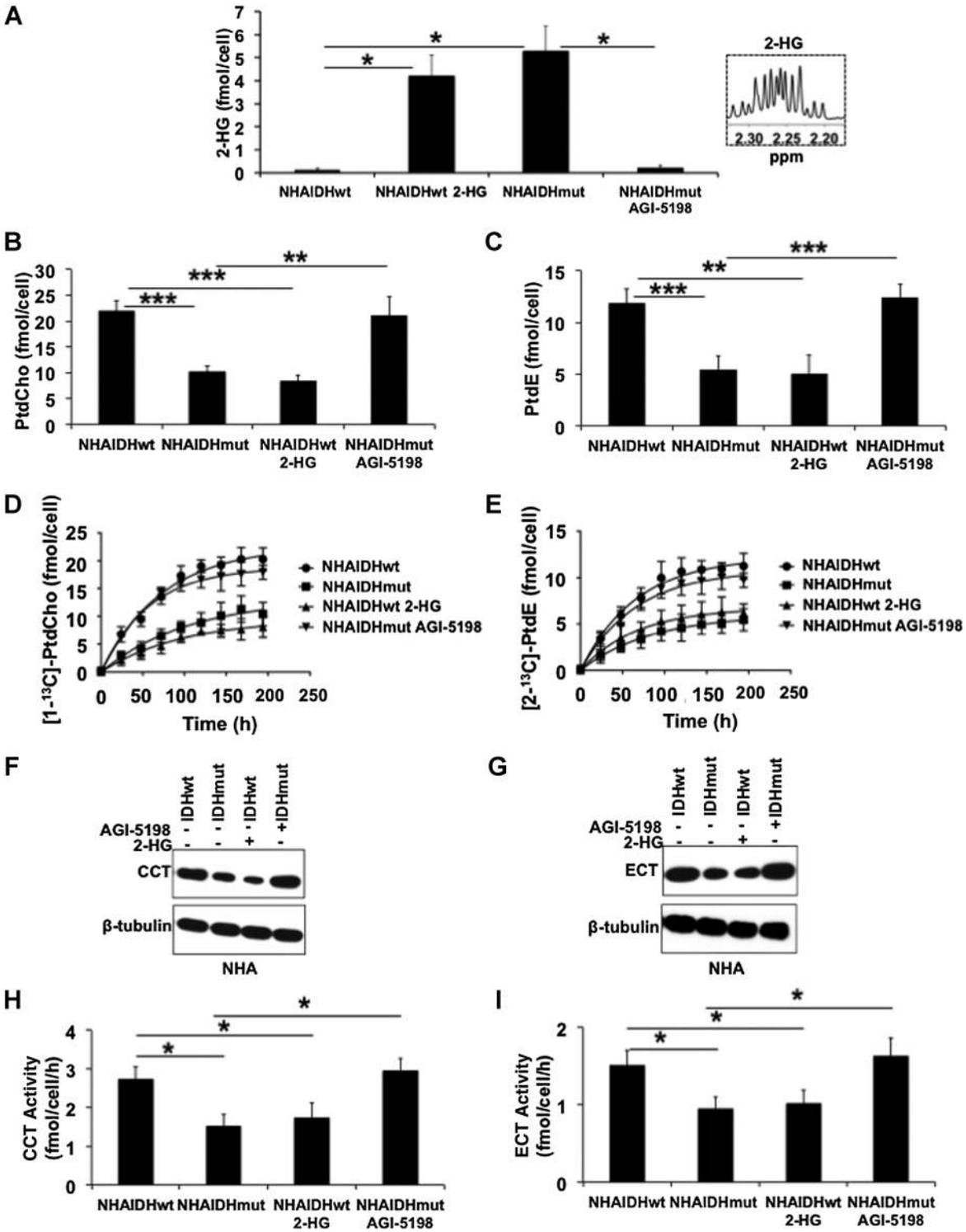

Figure 2.

2-HG downregulates PtdCho and PtdE biosynthesis. **A,** Intracellular 2-HG levels in NHAIDHwt, NHAIDHwt incubated with 2-HG, NHAIDHmut and NHAIDHmut treated with AGI-5198. The inset shows a ^{1}H-MR spectrum of 2-HG (2.19–2.30 ppm). Effect of 2-HG on steady-state PtdCho (**B**), steady-state PtdE (**C**), [1-^{13}C]-PtdCho synthesis (**D**), and [2-^{13}C]-PtdE synthesis (**E**) in the NHA model. Representative Western blots showing the effect of 2-HG on CCT (**F**) and ECT (**G**) expression in the NHA model. The bands for NHAIDHwt and NHAIDHmut are identical to those in Fig. 1, because they were part of the same experiment. Effect of 2-HG on CCT (**H**) and ECT (**I**) activity in the NHA model. *, $P < 0.05$; **, $P < 0.01$; ***, $P < 0.005$.

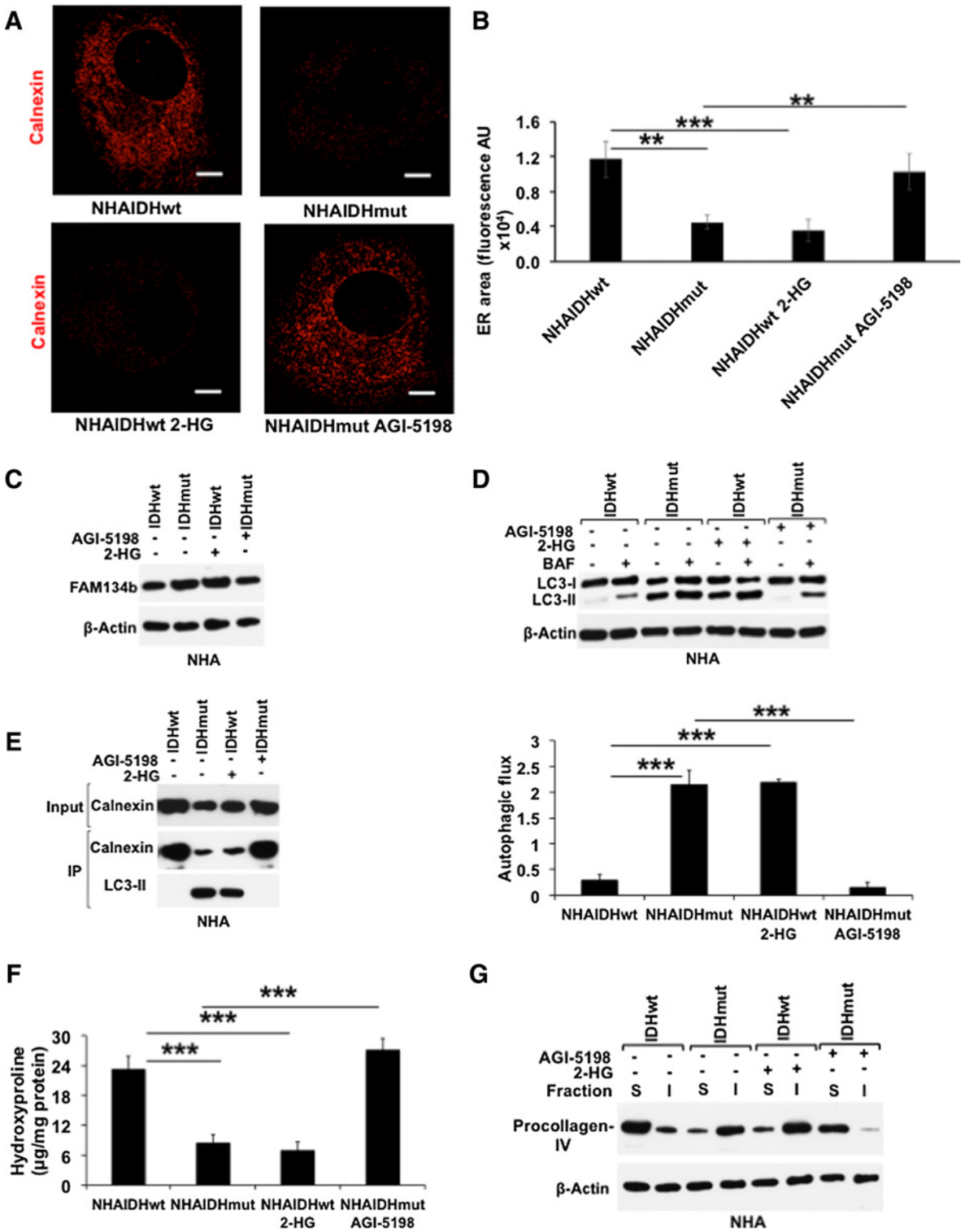

Figure 3.

2-HG induces ER-phagy in IDHmut glioma cells. **A,** Super-resolution STORM imaging of ER area in the NHA model. Scale bar, 5 µm. **B,** Quantification of ER area in the NHA model. **C,** Western blots of FAM134b in the NHA model. **D,** Western blots (top) showing autophagic flux with quantification (bottom) for the NHA model. **E,** Western blots showing the effect of 2-HG on coimmunoprecipitation of LC3-II with calnexin in the NHA model. **F,** Effect of 2-HG on hydroxyproline levels in the NHA model. **G,** Western blots showing procollagen-IV in detergent-soluble and -insoluble fractions in the NHA model. **, $P < 0.01$; ***, $P < 0.005$.

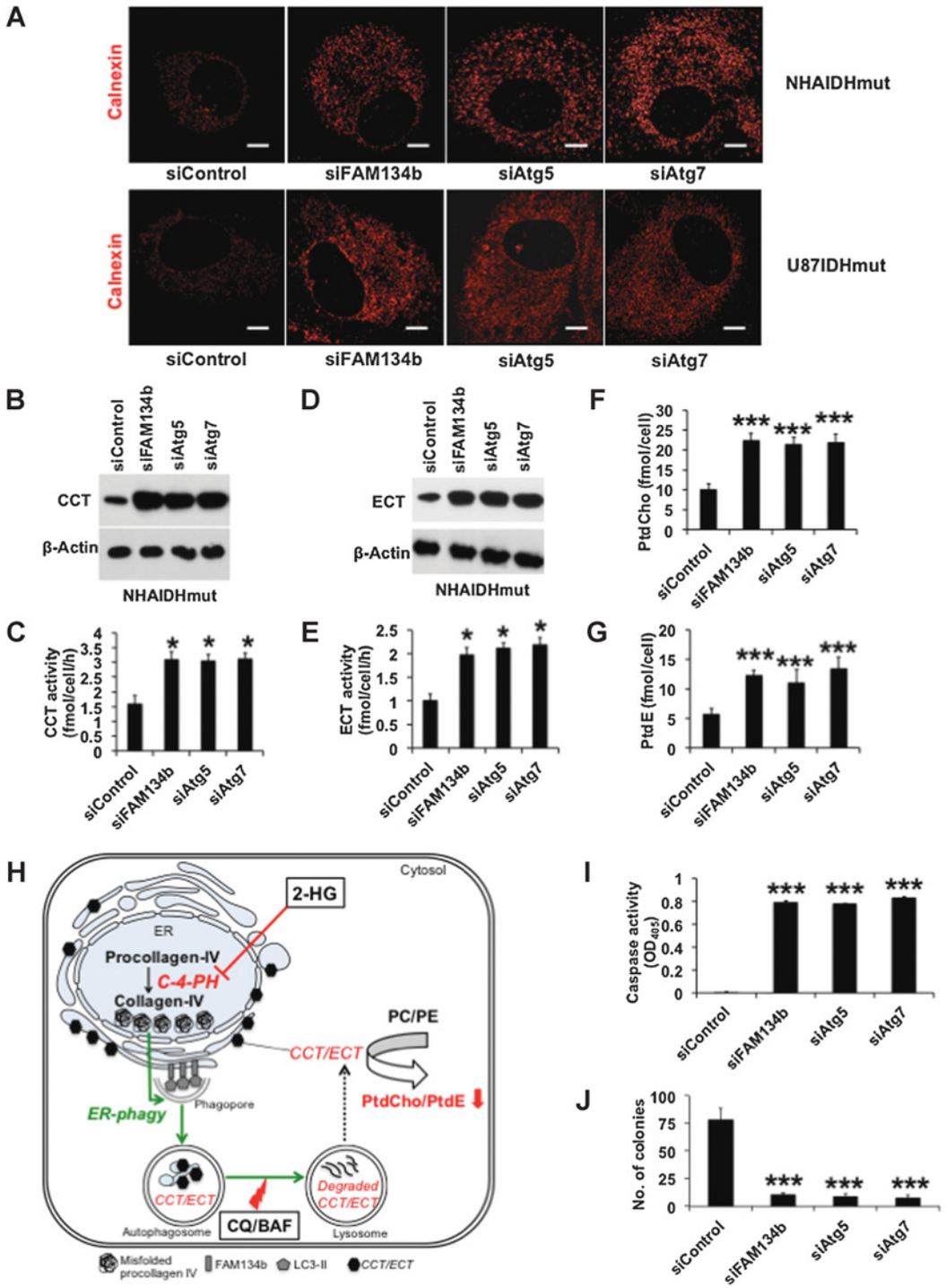

Figure 4.

Silencing FAM134b, Atg5, or Atg7 restores phospholipid biosynthesis in IDHmut glioma cells. **A,** Effect of FAM134b/Atg5/Atg7 silencing on the ER area in the NHA (top) and U87 (bottom) models visualized by STORM imaging. Scale bar, 5 μm. Effect of FAM134b/Atg5/Atg7 silencing on CCT expression (**B**), CCT activity (**C**), ECT expression (**D**), ECT activity (**E**), PtdCho (**F**), and PtdE (**G**) in the NHA model. **H,** Schematic illustration of the mechanism by which 2-HG downregulates phospholipid biosynthesis. 2-HG inhibits collagen-4-prolyl hydroxylase (C-4-PH) activity, leading to accumulation of misfolded procollagen-IV and triggering ER-phagy. The resulting turnover of the ER and degradation of CCT and ECT leads to reduced PtdCho and PtdE biosynthesis and steady-state levels. CQ and BAF are late-stage autophagy inhibitors that prevent degradation of autophagic cargo. Processes upregulated by 2-HG are highlighted in green. Metabolites/enzymes downregulated by 2-HG are highlighted in red. Effect of FAM134b/Atg5/Atg7 silencing on caspase activity (**I**) and clonogenicity (**J**) in the NHA model. *, $P < 0.05$; ***, $P < 0.005$.

Pharmacologically inhibiting autophagy abrogates clonogenicity of IDHmut glioma cells

To assess the therapeutic potential of pharmacologically inhibiting autophagy, we examined the effect of the late-stage autophagy inhibitors CQ and BAF on IDHmut cells. Both agents significantly increased accumulation of detergent-insoluble misfolded procollagen-IV (Fig. 5A; Supplementary Fig. S6A) and induced ER expansion (Fig. 5B). Concomitantly, CQ and BAF increased CCT activity, ECT activity, PtdCho, and PtdE in both NHAIDHmut (Fig. 5C–F) and U87IDHmut (Supplementary Fig. S6B–S6E) cells. Importantly, CQ and BAF induced caspase activity (Fig. 5G; Supplementary Fig. S6F) and inhibited clonogenicity (Fig. 5H; Supplementary Fig. S6G). The impact of treatment on clonogenicity (Supplementary Fig. S6H–S6I) and phospholipid levels (Supplementary Fig. S6J–S6M) was time dependent.

Because CQ and BAF are general autophagy inhibitors rather than specific ER-phagy inhibitors, we also examined their effect on IDHwt cells. CQ and BAF did not alter ER area, CCT activity, ECT activity, PtdCho, or PtdE in NHAIDHwt or U87IDHwt cells (Supplementary Fig. S7A–S7I). Furthermore, and importantly, CQ and BAF did not affect clonogenicity of NHAIDHwt cells (Supplementary Fig. S7J). In the U87IDHwt model, CQ and BAF did inhibit clonogenicity (Supplementary Fig. S7K), consistent with the glioblastoma background of this model and the known impact of autophagy inhibitors in glioblastoma (42). Nonetheless, the impact of CQ and BAF in U87IDHwt cells was significantly less than that observed in U87IDHmut cells (27% for CQ in U87IDHwt vs. 63% in U87IDHmut, $P < 0.01$ and 29% for BAF in U87IDHwt vs. 58% in U87IDHmut, $P < 0.01$; compare Supplementary Fig. S7K with Supplementary Fig. S6G). Caspase activity was also below detection in CQ-treated IDHwt cells. Taken together, our results indicated that IDHmut cells were vulnerable to disruption of autophagy, identifying a promising therapeutic strategy for these cells.

ER-phagy downregulates phospholipid biosynthesis in the BT54 patient–derived IDHmut glioma model

Next, we wanted to confirm our findings in a clinically relevant IDHmut model. To that end, we examined BT54 neurospheres that are derived from an oligodendroglioma tumor carrying an IDH1 mutation (Supplementary Fig. S8A; ref. 27) and that produce 2-HG as determined by ^{1}H-MRS (6.2±0.1 fmol/cell). In line with our results with the genetically engineered models, silencing FAM134b/Atg5/Atg7 (Supplementary Fig. S8B) abrogated coimmunoprecipitation of LC3-II with calnexin (Supplementary Fig. S8C). Concomitantly, ER area (Fig. 6A), CCT activity (Fig. 6B), ECT activity (Fig. 6C), PtdCho (Fig. 6D), and PtdE (Fig. 6E) increased. Silencing autophagy also induced caspase activity (Fig. 6F) and inhibited BT54 cell proliferation (Fig. 6G). Likewise, treating BT54 neurospheres with CQ and BAF increased ER area (Fig. 6H), CCT activity (Fig. 6I), ECT activity (Fig. 6J), PtdCho (Fig. 6K), and PtdE (Fig. 6L). At the same time, caspase activity (Fig. 6M) was observed, indicating induction of apoptosis, and BT54 proliferation was inhibited (Fig. 6N).

Inhibition of ER-phagy restores phospholipid levels and inhibits growth of orthotopic U87IDHmut gliomas *in vivo*

Next, we wanted to confirm our findings *in vivo* and examined the effect of CQ on phospholipid levels and tumor growth in orthotopic U87IDHwt and U87IDHmut tumor xenografts. First, we established that LC3-II levels were higher in CQ-treated U87IDHwt (Supplementary Fig. S8D) and U87IDHmut (Fig. 7A) tumors relative to control, confirming that CQ blocked autophagosome turnover and inhibited autophagy in both models *in vivo*. Consistent with our results *in vitro*, CQ did not alter calnexin levels, CCT activity, ECT activity, or phospholipid levels in U87IDHwt tumor xenografts (Supplementary Fig. S8E–S8I). CQ treatment also did not result in detectable caspase activity in U87IDHwt tumors. In contrast, calnexin levels were higher in CQ-treated U87IDHmut tumors relative to controls (Fig. 7B), indicating ER expansion, and caspase activity (Fig. 7C), indicating induction of apoptosis, was observed in CQ-treated U87IDHmut tumors. Furthermore, CCT activity, ECT activity, PtdCho, and PtdE (Fig. 7D–G) were also higher in CQ-treated U87IDHmut tumors, confirming the link between ER-phagy and phospholipid biosynthesis in IDHmut gliomas *in vivo*. Finally, examination of T2-weighted MR images from control and CQ-treated animals (Fig. 7H; Supplementary Fig. S8J) indicated that, consistent with our findings in cells, CQ significantly inhibited tumor growth in both U87IDHwt and U87IDHmut models (by 46%, $P < 0.01$, for U87IDHwt and by 58%, $P < 0.005$, for U87IDHmut at D7 of treatment, Fig. 7I). Inhibition of tumor growth was associated with enhanced survival from an average of 13 ± 4 days in controls to at least 21 days in treated animals (the time point at which all animals were sacrificed for further investigation of tumor tissue). However, as in the cell study, U87IDHmut tumors appeared potentially more sensitive to treatment than U87IDHwt tumors. Specifically, at D7 from start of treatment, control U87IDHwt and U87IDHmut tumors were not significantly different in volume (303% ± 65% of D0 for U87IDHwt and 225% ± 26% of D0 for U87IDHmut, $P = 0.21$). However, CQ-treated U87IDHmut tumor volume was comparable with values at D0 and significantly different from U87IDHwt tumor volume (101% ± 22% for U87IDHmut and 163% ± 21% for U87IDHwt, $P < 0.005$; Fig. 7I). Similarly, at D21 CQ-treated U87IDHmut tumors had shrunk to a volume of 74% ± 15% of D0 while U87IDHwt tumors measured 141% ± 11% of D0 ($P < 0.005$).

Phospholipid biosynthesis is downregulated in IDHmut glioma patient biopsies

Finally, to determine if our findings were applicable to human patients, we examined IDHwt and IDHmut glioma patient biopsies. Consistent with the data in cell models, Western blotting showed higher levels of FAM134b (Fig. 7J; Supplementary Fig. S8K) and LC3-II (Fig. 7K; Supplementary Fig. S8L) in IDHmut biopsies relative to IDHwt. LC3-II levels were also higher in IDHmut biopsies as determined by immunohistochemistry (Fig. 7L). Concomitantly, calnexin (Fig. 7M; Supplementary Fig. S8M) levels were lower in IDHmut biopsies relative to IDHwt. Importantly, we observed a significant reduction in CCT activity (40%; Fig. 7N), ECT activity (43%, Fig. 7O), PtdCho (50%, Fig. 7P), and PtdE (63%, Fig. 7Q) in IDHmut patient biopsies relative to IDHwt.

Discussion

Our study delineates a previously unrecognized role for 2-HG in downregulating phospholipid biosynthesis in IDHmut gliomas. Using genetically engineered and patient-derived cell models, we demonstrate that this downregulation is mediated via ER-phagy. Importantly, inhibition of ER-phagy triggers apoptosis and significantly attenuates tumor growth in a preclinical IDHmut glioma model. Furthermore, we observed ER-phagy and

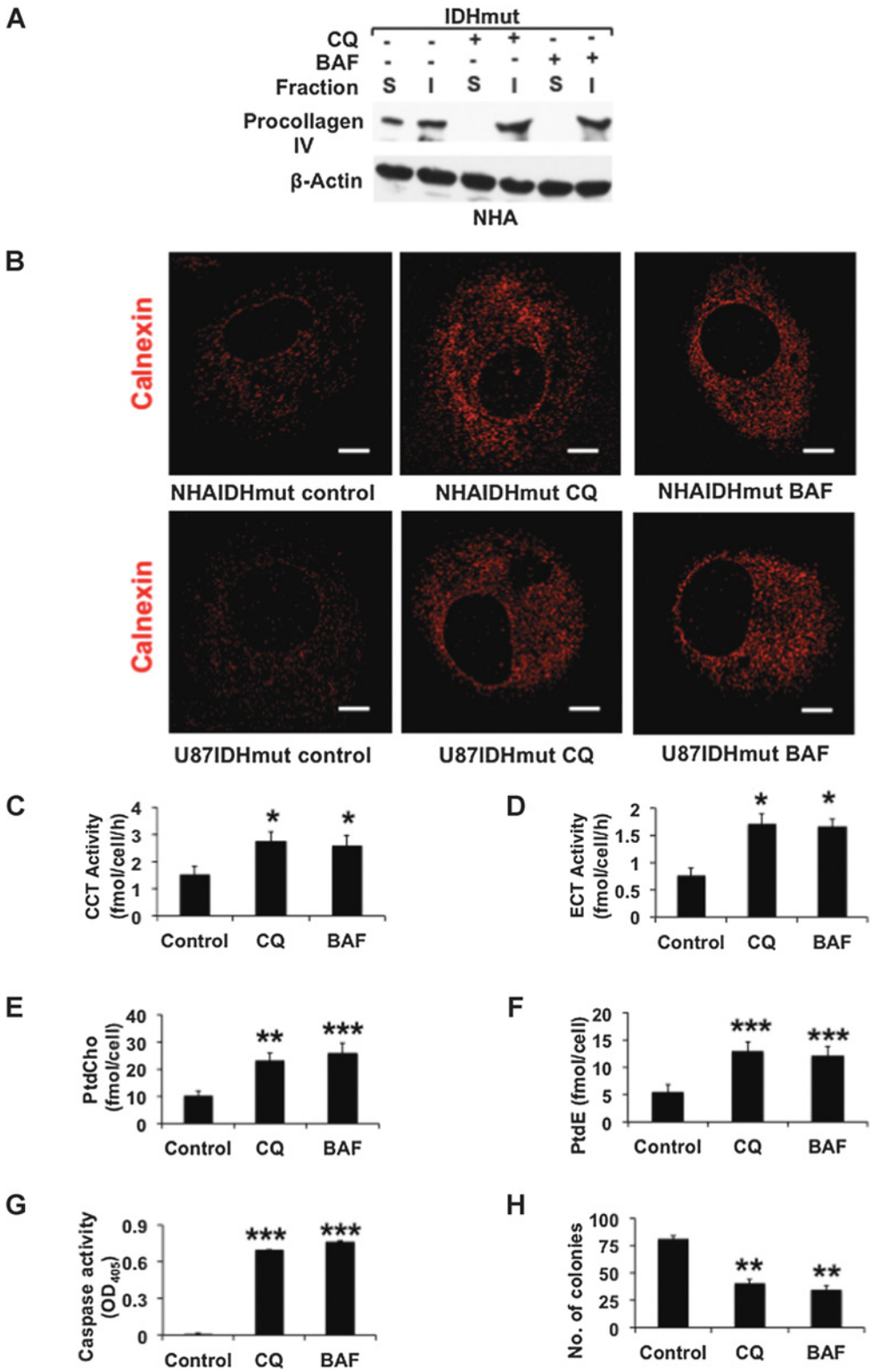

Figure 5.

CQ and BAF restore phospholipid levels and inhibit clonogenicity of IDHmut glioma cells. Western blots showing procollagen-IV in detergent-soluble and -insoluble fractions following CQ and BAF treatment in the NHA (**A**) model. **B,** Effect of CQ and BAF on ER area in the NHA (top) and U87 (bottom) models. Scale bar, 5 μm. Effect of CQ and BAF on CCT activity (**C**), ECT activity (**D**), PtdCho (**E**), PtdE (**F**), caspase activity (**G**), and clonogenicity (**H**) in the NHA model. *, $P < 0.05$; **, $P < 0.01$; ***, $P < 0.005$.

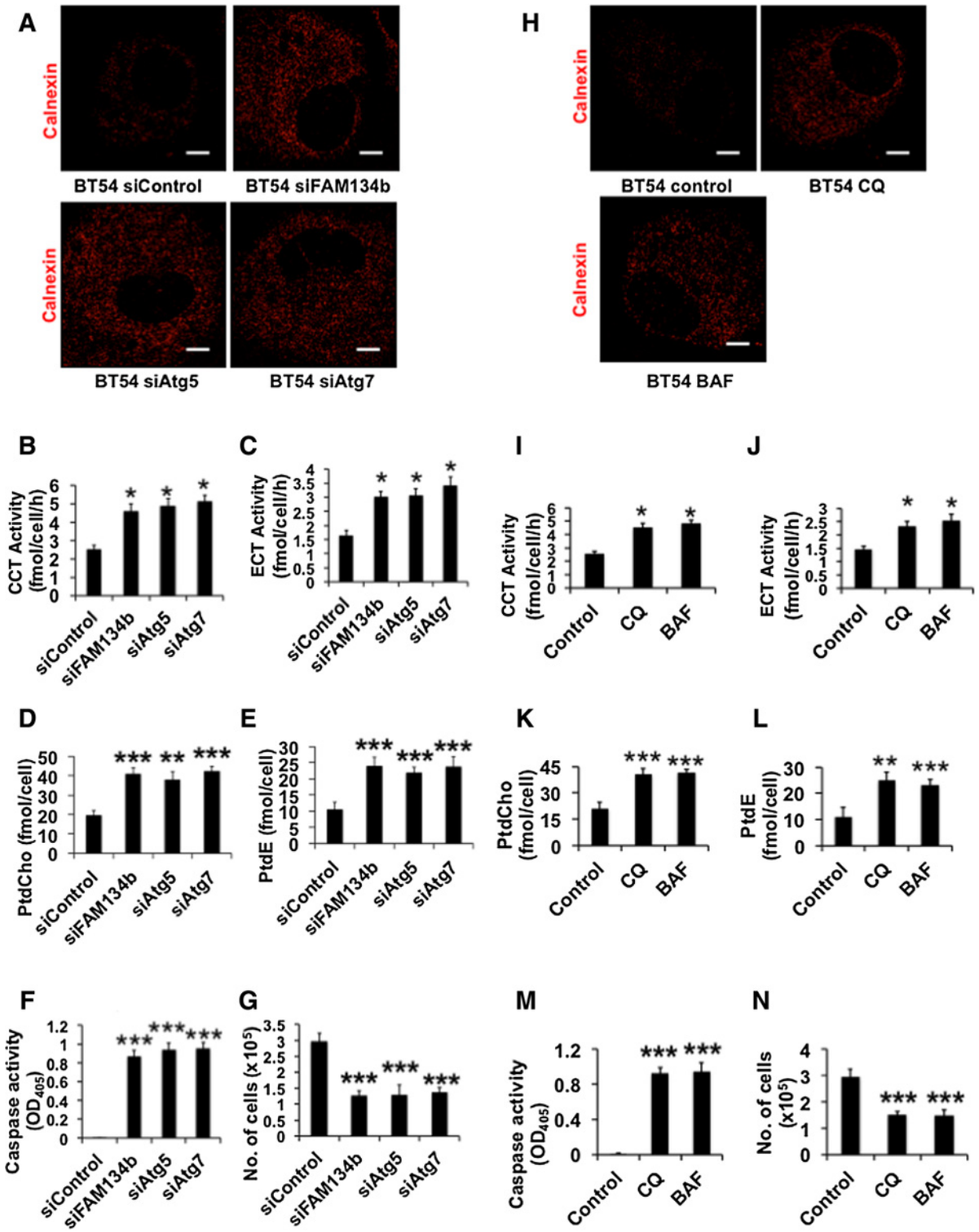

Figure 6.

ER-phagy downregulates phospholipid biosynthesis in the BT54 patient-derived IDHmut model. Effect of FAM134b/Atg5/Atg7 silencing on ER area (**A**), CCT activity (**B**), ECT activity (**C**), PtdCho (**D**), PtdE (**E**), caspase activity (**F**), and cell proliferation (**G**) in the BT54 model. Effect of CQ and BAF on ER area (**H**), CCT activity (**I**), ECT activity (**J**), PtdCho (**K**), PtdE (**L**), caspase activity (**M**), and cell proliferation (**N**) in BT54 neurospheres. Scale bar for STORM images, 5 μm. *, $P < 0.05$; **, $P < 0.01$; ***, $P < 0.005$.

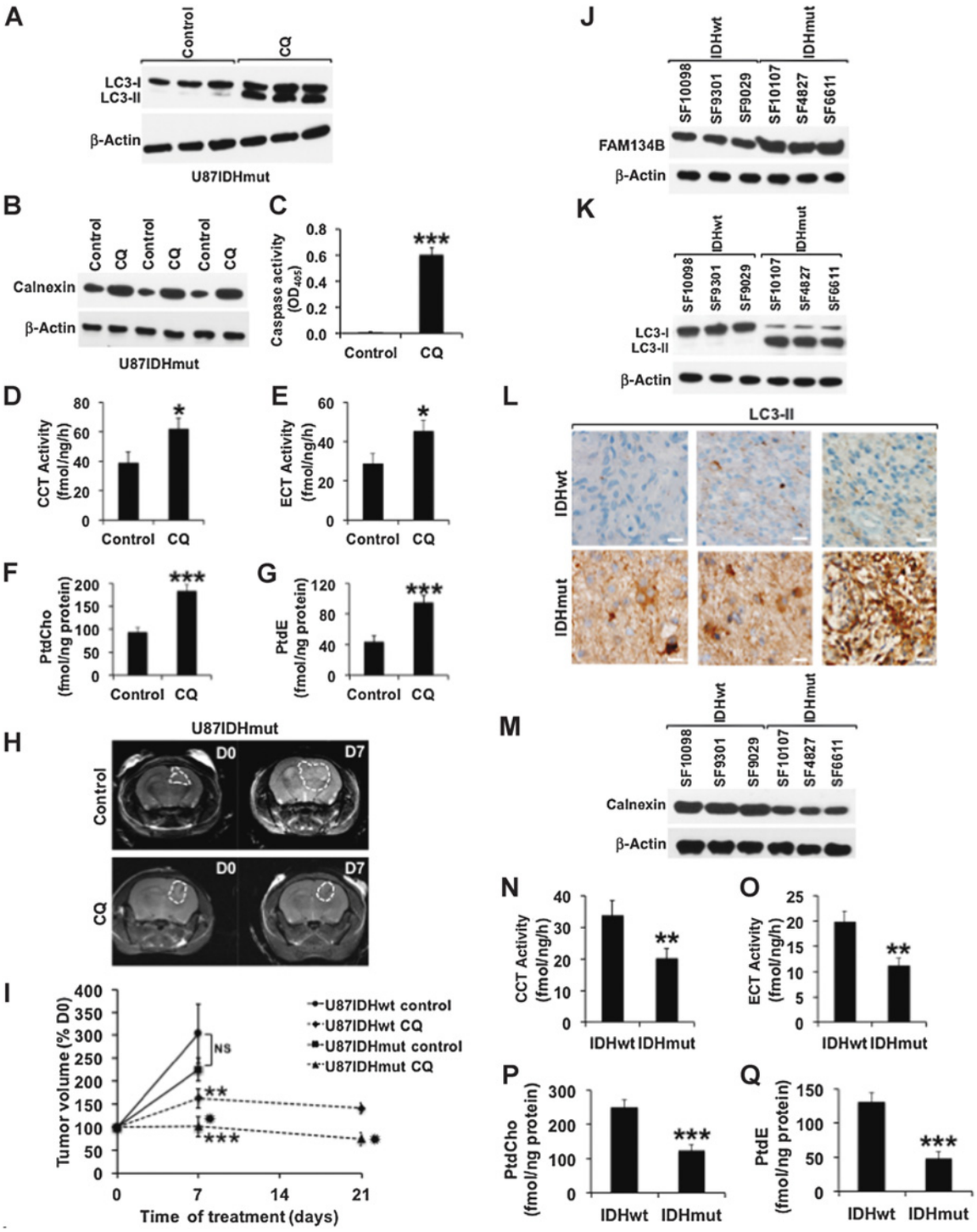

Figure 7.

Phospholipid biosynthesis is downregulated in orthotopic IDHmut tumor xenografts (**A–I**) and IDHmut glioma patient biopsies (**J–Q**). LC3-II (**A**), calnexin (**B**), caspase activity (**C**), CCT activity (**D**), ECT activity (**E**), PtdCho (**F**), and PtdE (**G**) in control and CQ-treated U87IDHmut tumors. **H,** Representative T2-weighted MR images of U87IDHmut orthotopic tumor-bearing mice treated with saline or CQ at day 0 (D0) and day 7 (D7). The tumor is contoured in white. **I,** Tumor volume at D0, D7, and D21 in control and CQ-treated U87IDHwt and U87IDHmut tumor xenografts. NS, difference is not statistically significant. *, statistical significance for CQ-treated tumors relative to control (**, $P < 0.01$; ***, $P < 0.005$). ⁎, statistical significance between CQ-treated U87IDHmut and CQ-treated U87IDHwt tumors at the same time point. Western blots for FAM134b (**J**) and LC3-II (**K**), immunohistochemical staining for LC3-II (**L**), Western blots for calnexin (**M**), CCT activity (**N**), ECT activity (**O**), PtdCho (**P**), and PtdE (**Q**) in IDHwt and IDHmut glioma patient biopsies. Scale bar, 50 μm.

downregulation of phospholipid levels in IDHmut glioma patient biopsies, highlighting the translational validity of our findings. Overall, these findings expand our understanding of the metabolic reprogramming induced by 2-HG and its functional consequences for IDHmut glioma proliferation.

Previous studies demonstrated that PC and PE, the precursors of PtdCho and PtdE, were reduced in IDHmut glioma cells relative to IDHwt (24–26). We extend these findings to show that PtdCho and PtdE are also reduced. We also show that the drop in phospholipids is linked to 2-HG via ER-phagy-mediated reduction in CCT and ECT and, consistent with this mechanism, silencing ER-phagy restores CCT and ECT expression and activity, as well as phospholipid biosynthesis. Our results are in line with previous studies demonstrating that CCT and ECT are the rate-limiting and regulatory enzymes in phospholipid biosynthesis and that their inhibition is sufficient to inhibit phospholipid biosynthesis (14, 18). However, it is important to note that in cancer cells choline kinase and ethanolamine kinase, the enzymes catalyzing PC and PE synthesis, can be rate limiting for phospholipid synthesis (18). While CCT and ECT are localized to the ER, choline kinase, and ethanolamine kinase are cytosolic (14, 18). Further studies are therefore needed to assess whether these enzymes might also be playing a role in modulating phospholipid synthesis and, conversely, whether ER-phagy might play a role in explaining the reduction in PC and PE levels in IDHmut gliomas.

We find that 2-HG triggers increased autophagic flux in our models. These findings are consistent with a prior study demonstrating that 2-HG triggers autophagy in U87 cells (43). The same study, however, did not find any difference in LC3-II levels between IDHwt and IDHmut glioma patient biopsies, in contrast to our observations. Detection of endogenous LC3-II in tissue samples is problematic and studies have recommended the Nanotools antibody 5F10 that was used in the current study for unambiguous detection (44, 45). It is possible that the difference between our study and that of Gilbert et al. stems from the use of different antibodies. Our study also indicates that FAM134b expression, which is specific to autophagy of the ER, is higher in IDHmut cells relative to IDHwt, a finding that was also observed in our IDHmut patient biopsies and that links the IDH1 mutation to ER-phagy. Nonetheless, further studies with a larger cohort of patient samples are needed to confirm our observations linking 2-HG to ER-phagy.

While we cannot exclude the possibility of other stressors, our results indicate that ER-phagy is triggered in response to the accumulation of misfolded procollagen-IV. The observation that treating IDHwt cells with the prolyl hydroxylase inhibitor EDHB induces misfolded procollagen-IV accumulation and triggers ER-phagy strengthens the link between inhibition of C-4-PH activity and ER-phagy. Within IDHmut cells, C-4-PH activity is likely inhibited by 2-HG as reported in previous studies (37, 38), with 2-HG acting as a competitive inhibitor of α-KG, which is essential for C-4-PH activity (46). Inspection of patient biopsy data from the TCGA database did not show changes in expression of any of the genes coding for C-4-PH (P4HA1, P4HA2, and P4HA3, which code for the α subunit, and P4HB, which codes for the β subunit) when comparing IDHwt and IDHmut tumors (Supplementary Fig. S8N–S8Q), ruling out changes in C-4-PH expression as an explanation for our findings.

Our study identifies a role for ER-phagy in enabling survival of IDHmut gliomas. Autophagy is often described as a "double-edged sword" that can suppress or aid tumorigenesis in a context-dependent manner (47). 2-HG–mediated collagen-IV misfolding has been shown to induce ER-stress–mediated apoptosis in the brains of IDHmut knock-in mice, resulting in embryonic lethality (39). In contrast, our findings suggest that IDHmut cells induce ER-phagy in response to misfolded procollagen-IV accumulation. It is possible that IDHmut gliomas have evolved to activate ER-phagy as a means of avoiding apoptotic cell death. The observation that inhibiting ER-phagy increases accumulation of misfolded procollagen-IV and induces apoptosis lends support to this prosurvival role of ER-phagy.

Our study indicates that inhibiting ER-phagy is a novel therapeutic opportunity for IDHmut gliomas. Due to the lack of pharmacological inhibitors of ER-phagy, we used CQ to inhibit ER-phagy at the lysosomal stage. Following CQ treatment, *in vitro* clonogenicity and *in vivo* tumor growth were inhibited to a greater extent in IDHmut gliomas compared with IDHwt and this effect was associated with increased phospholipid levels in IDHmut, but not IDHwt, gliomas. These findings provide proof-of-concept in a preclinical model that targeting ER-phagy is a viable therapeutic option for IDHmut gliomas. They also provide a rational basis for clinical trials such as NCT02496741 exploring the efficacy of combination CQ and metformin treatment in IDHmut gliomas (48). Importantly, our finding that silencing FAM134b induces apoptotic cell death and inhibits proliferation of IDHmut cells indicates that identifying small-molecule inhibitors of FAM134b could be a potential avenue for drug discovery specific to IDHmut glioma.

Our study is the first demonstration of oncometabolite-driven downregulation of phospholipid biosynthesis in cancer. In addition to their structural role as membrane components, phospholipids also play key roles in signal transduction and cell–cell interactions (11, 15). As a result, phospholipid levels are usually upregulated during malignant transformation (12–15) including in glioblastoma compared with normal brain (49). Primary glioblastoma are typically IDHwt, high-grade, fast-growing, and aggressive, whereas primary oligodendroglioma and astrocytoma are mostly IDHmut, lower-grade, slower growing, and less aggressive. Consistent with our findings, an earlier small-scale study reported higher PtdCho levels in higher-grade brain tumors compared with lower grade (49). Further studies are needed to assess how phospholipid synthesis might be altered when tumors recur and upgrade. Nonetheless, it is tempting to speculate that reduced phospholipid biosynthesis in IDHmut gliomas is linked to the slower rate of proliferation of these tumors when compared with IDHwt glioblastoma (50).

To the best of our knowledge, this investigation is the first to demonstrate a functional link between ER-phagy and phospholipid metabolism in cancer. While autophagy has been linked to several metabolic processes including glycolysis, glutaminolysis, tricarboxylic acid cycle, and fatty acid metabolism (41), the investigation of ER-phagy has primarily focused on its role in counterbalancing ER stress due to protein misfolding. Our data indicate that downregulation of phospholipid biosynthesis, while linked to protein misfolding, is also a unique metabolic outcome of ER-phagy in IDHmut gliomas.

In summary, our studies shed light on fundamental aspects of glioma biology by highlighting the unique crosstalk between 2-HG and ER-phagy in the control of phospholipid biosynthesis in IDHmut gliomas. Additionally, similar to previous studies (6–8), they highlight the therapeutic value of targeting 2-HG–driven metabolic reprogramming for treatment of IDHmut gliomas.

Disclosure of Potential Conflicts of Interest

No potential conflicts of interest were disclosed.

Authors' Contributions

Conception and design: P. Viswanath, J.L. Izquierdo-Garcia, S.M. Ronen
Development of methodology: P. Viswanath, R.O. Pieper, J.J. Phillips, S.M. Ronen
Acquisition of data (provided animals, acquired and managed patients, provided facilities, etc.): P. Viswanath, M. Radoul, J.L. Izquierdo-Garcia, W.Q. Ong, H.A. Luchman, J.G. Cairncross, J.J. Phillips
Analysis and interpretation of data (e.g., statistical analysis, biostatistics, computational analysis): P. Viswanath, M. Radoul, W.Q. Ong, S.M. Ronen
Writing, review, and/or revision of the manuscript: P. Viswanath, J.L. Izquierdo-Garcia, W.Q. Ong, J.G. Cairncross, B. Huang, R.O. Pieper, J.J. Phillips, S.M. Ronen
Administrative, technical, or material support (i.e., reporting or organizing data, constructing databases): P. Viswanath, W.Q. Ong
Study supervision: P. Viswanath, B. Huang, S.M. Ronen

Acknowledgments

The authors thank Prof. Jayanta Debnath (UCSF) for his insightful comments about the manuscript. We also thank Anne Marie Gillespie and Yunita Lim for technical support. This work was supported by the following grants: NIH R01CA172845 (S.M. Ronen), NIH R01CA197254 (S.M. Ronen), NIH R01CA154915 (S.M. Ronen), NIH DP2OD008479 (B. Huang), NIH U19CA179512 (B. Huang), NIH P50CA97257 (UCSF Brain Tumor Research Center SPORE Tissue Core to S.M. Ronen, R.O. Pieper, and J.J. Phillips), NIH P50CA97257 (Career Development Grant to P. Viswanath), Spanish Ministry of Economy, Industry and Competitiveness (MEIC-AEI) grants FP7/2007-2013 REA600396 and SAF2014-59118-JIN (J.L. Izquierdo-Garcia), charitable donations (UCSF Brain Tumor Loglio Collective to S.M. Ronen, R.O. Pieper, and J.J. Phillips; NICO to S.M. Ronen; UCSF Program for Breakthrough Biomedical Research to B. Huang).

The costs of publication of this article were defrayed in part by the payment of page charges. This article must therefore be hereby marked *advertisement* in accordance with 18 U.S.C. Section 1734 solely to indicate this fact.

Received September 22, 2017; revised December 8, 2017; accepted January 17, 2018; published first January 22, 2018.

References

1. Dang L, Su SM. Isocitrate dehydrogenase mutation and (R)-2-Hydroxyglutarate: from basic discovery to therapeutics development. Annu Rev Biochem 2017;86:305–331.
2. Wahl DR, Venneti S. 2-Hydoxyglutarate: D/Riving Pathology in gLiomaS. Brain Pathol 2015;25:760–8.
3. Viswanath P, Chaumeil MM, Ronen SM. Molecular imaging of metabolic reprograming in mutant IDH cells. Front Oncol 2016;6:60.
4. Viswanath P, Najac C, Izquierdo-Garcia JL, Pankov A, Hong C, Eriksson P, et al. Mutant IDH1 expression is associated with down-regulation of monocarboxylate transporters. Oncotarget 2016;7:34942–55.
5. Chesnelong C, Chaumeil MM, Blough MD, Al-Najjar M, Stechishin OD, Chan JA, et al. Lactate dehydrogenase A silencing in IDH mutant gliomas. Neuro Oncol 2014;16:686–95.
6. Izquierdo-Garcia JL, Viswanath P, Eriksson P, Cai L, Radoul M, Chaumeil MM, et al. IDH1 mutation induces reprogramming of pyruvate metabolism. Cancer Res 2015;75:2999–3009.
7. Seltzer MJ, Bennett BD, Joshi AD, Gao P, Thomas AG, Ferraris DV, et al. Inhibition of glutaminase preferentially slows growth of glioma cells with mutant IDH1. Cancer Res 2010;70:8981–7.
8. Tateishi K, Wakimoto H, Iafrate AJ, Tanaka S, Loebel F, Lelic N, et al. Extreme vulnerability of IDH1 mutant cancers to NAD+ depletion. Cancer Cell 2015;28:773–84.
9. Vance JE. Phospholipid synthesis and transport in mammalian cells. Traffic 2015;16:1–18.
10. van Meer G, Voelker DR, Feigenson GW. Membrane lipids: where they are and how they behave. Nat Rev Mol Cell Biol 2008;9:112–24.
11. Wenk MR. The emerging field of lipidomics. Nat Rev Drug Discov 2005;4:594–610.
12. Cheng M, Bhujwalla ZM, Glunde K. Targeting phospholipid metabolism in cancer. Front Oncol 2016;6:266.
13. Jackowski S. Coordination of membrane phospholipid synthesis with the cell cycle. J Biol Chem 1994;269:3858–67.
14. Lykidis A, Jackowski S. Regulation of mammalian cell membrane biosynthesis. Prog Nucleic Acid Res Mol Biol 2001;65:361–93.
15. Ridgway ND. The role of phosphatidylcholine and choline metabolites to cell proliferation and survival. Crit Rev Biochem Mol Biol 2013;48:20–38.
16. Gibellini F, Smith TK. The Kennedy pathway–De novo synthesis of phosphatidylethanolamine and phosphatidylcholine. IUBMB Life 2010;62:414–28.
17. Arlauckas SP, Popov AV, Delikatny EJ. Choline kinase alpha-Putting the ChoK-hold on tumor metabolism. Prog Lipid Res 2016;63:28–40.
18. Kent C. Regulation of phosphatidylcholine biosynthesis. Prog Lipid Res 1990;29:87–105.
19. Cornell RB, Northwood IC. Regulation of CTP: phosphocholine cytidylyltransferase by amphitropism and relocalization. Trends Biochem Sci 2000;25:441–7.
20. Vance JE, Vance DE. Phospholipid biosynthesis in mammalian cells. Biochem Cell Biol 2004;82:113–28.
21. Daly PF, Lyon RC, Faustino PJ, Cohen JS. Phospholipid metabolism in cancer cells monitored by 31P NMR spectroscopy. J Biol Chem 1987;262:14875–78.
22. McKnight TR, Noworolski SM, Vigneron DB, Nelson SJ. An automated technique for the quantitative assessment of 3D-MRSI data from patients with glioma. J Magn Reson Imaging 2001;13:167–77.
23. Glunde K, Bhujwalla ZM. Metabolic tumor imaging using magnetic resonance spectroscopy. Semin Oncol 2011;38:26–41.
24. Reitman ZJ, Jin G, Karoly ED, Spasojevic I, Yang J, Kinzler KW, et al. Profiling the effects of isocitrate dehydrogenase 1 and 2 mutations on the cellular metabolome. Proc Natl Acad Sci U S A 2011;108:3270–5.
25. Izquierdo-Garcia JL, Viswanath P, Eriksson P, Chaumeil MM, Pieper RO, Phillips JJ, et al. Metabolic reprogramming in mutant IDH1 glioma cells. PLoS One 2015;10:e0118781.
26. Esmaeili M, Hamans BC, Navis AC, van Horssen R, Bathen TF, Gribbestad IS, et al. IDH1 R132H mutation generates a distinct phospholipid metabolite profile in glioma. Cancer Res 2014;74:4898–907.
27. Kelly JJ, Blough MD, Stechishin OD, Chan JA, Beauchamp D, Perizzolo M, et al. Oligodendroglioma cell lines containing t(1;19)(q10;p10). Neuro Oncol 2010;12:745–55.
28. Ward CS, Eriksson P, Izquierdo-Garcia JL, Brandes AH, Ronen SM. HDAC inhibition induces increased choline uptake and elevated phosphocholine levels in MCF7 breast cancer cells. PLoS One 2013;8:e62610.
29. Huang B, Wang W, Bates M, Zhuang X. Three-dimensional super-resolution imaging by stochastic optical reconstruction microscopy. Science 2008;319:810–3.
30. Berg RA. Determination of 3- and 4-hydroxyproline. Methods Enzymol 1982;82 Pt A:372–98.
31. Rohle D, Popovici-Muller J, Palaskas N, Turcan S, Grommes C, Campos C, et al. An inhibitor of mutant IDH1 delays growth and promotes differentiation of glioma cells. Science 2013;340:626–30.
32. Fagone P, Jackowski S. Membrane phospholipid synthesis and endoplasmic reticulum function. J Lipid Res 2009;50:S311–6.
33. Khaminets A, Heinrich T, Mari M, Grumati P, Huebner AK, Akutsu M, et al. Regulation of endoplasmic reticulum turnover by selective autophagy. Nature 2015;522:354–8.
34. Bernales S, McDonald KL, Walter P. Autophagy counterbalances endoplasmic reticulum expansion during the unfolded protein response. PLoS Biol 2006;4:e423.
35. Fumagalli F, Noack J, Bergmann TJ, Cebollero E, Pisoni GB, Fasana E, et al. Translocon component Sec62 acts in endoplasmic reticulum turnover during stress recovery. Nat Cell Biol 2016;18:1173–84.

36. Klionsky DJ, Abdelmohsen K, Abe A, Abedin MJ, Abeliovich H, Acevedo Arozena A, et al. Guidelines for the use and interpretation of assays for monitoring autophagy (3rd edition). Autophagy 2016; 12:1–222.
37. Xu W, Yang H, Liu Y, Yang Y, Wang P, Kim SH, et al. Oncometabolite 2-hydroxyglutarate is a competitive inhibitor of alpha-ketoglutarate-dependent dioxygenases. Cancer Cell 2011;19:17–30.
38. Sasaki M, Knobbe CB, Itsumi M, Elia AJ, Harris IS, Chio II, et al. D-2-hydroxyglutarate produced by mutant IDH1 perturbs collagen maturation and basement membrane function. Genes Dev 2012;26: 2038–49.
39. Sasaki T, Majamaa K, Uitto J. Reduction of collagen production in keloid fibroblast cultures by ethyl-3,4-dihydroxybenzoate. Inhibition of prolyl hydroxylase activity as a mechanism of action. J Biol Chem 1987;262: 9397–403.
40. Kadowaki H, Nishitoh H. Signaling pathways from the endoplasmic reticulum and their roles in disease. Genes (Basel) 2013; 4:306–33.
41. Guo JY, White E. Autophagy, metabolism, and cancer. Cold Spring Harb Symp Quant Biol 2016;81:73–78.
42. Kim EL, Wustenberg R, Rubsam A, Schmitz-Salue C, Warnecke G, Bucker EM, et al. Chloroquine activates the p53 pathway and induces apoptosis in human glioma cells. Neuro Oncol 2010;12:389–400.
43. Gilbert MR, Liu Y, Neltner J, Pu H, Morris A, Sunkara M, et al. Autophagy and oxidative stress in gliomas with IDH1 mutations. Acta Neuropathol 2014;127:221–33.
44. Rosenfeldt MT, Nixon C, Liu E, Mah LY, Ryan KM. Analysis of macroautophagy by immunohistochemistry. Autophagy 2012;8:963–9.
45. Martinet W, Schrijvers DM, Timmermans JP, Bult H, De Meyer GR. Immunohistochemical analysis of macroautophagy: recommendations and limitations. Autophagy 2013;9:386–402.
46. Rhoads RE, Udenfriend S. Decarboxylation of alpha-ketoglutarate coupled to collagen proline hydroxylase. Proc Natl Acad Sci U S A 1968;60:1473–8.
47. Thorburn A. Autophagy and its effects: making sense of double-edged swords. PLOS Biol 2014;12:e1001967.
48. Molenaar RJ, Coelen RJ, Khurshed M, Roos E, Caan MW, van Linde ME, et al. Study protocol of a phase IB/II clinical trial of metformin and chloroquine in patients with IDH1-mutated or IDH2-mutated solid tumours. BMJ Open 2017;7:e014961.
49. Lehnhardt FG, Rohn G, Ernestus RI, Grune M, Hoehn M. 1H- and (31)P-MR spectroscopy of primary and recurrent human brain tumors in vitro: malignancy-characteristic profiles of water soluble and lipophilic spectral components. NMR Biomed 2001;14:307–17.
50. Baldock AL, Yagle K, Born DE, Ahn S, Trister AD, Neal M, et al. Invasion and proliferation kinetics in enhancing gliomas predict IDH1 mutation status. Neuro Oncol 2014;16:779–86.